A novel antibacterial benzimidazolium hexachlorotellurate hybrid compound: Experimental-theoretical characterization

Fatma Bentahar [a,b], Mohammed S.M. Abdelbaky [a,b,*], M. Isabel Menéndez [b], Pedro Huidobro [c], Santiago García-Granda [b], Mohamed Dammak [a]

[a] *Laboratory Inorganic Chemistry, Faculty of Sciences of Sfax, University of Sfax, 3000 Sfax, Tunisia*
[b] *Department of Physical and Analytical Chemistry, Faculty of Chemistry, University of Oviedo-CINN, 33006 Oviedo, Spain*
[c] *Departament of Statistics and O.R, University of Oviedo, 33007 Oviedo, Spain*

ABSTRACT

Inspired by the antibacterial properties of recent hybrid materials containing hexahalogenotellurate anions, a novel hybrid compound, formulated as $(C_7H_7N_2)_2TeCl_6.(H_2O)_2$ (**T3**), was synthesized by slow evaporation from a mixture of tellurium dioxide and HCl added to a benzimidazole solution at room temperature. **T3** was fully characterized using various methods such as X-ray diffraction (SC-XRD & XRPD), Fourier-transform infrared spectroscopy (FT-IR), ultraviolet–visible spectroscopy (UV–Vis), Mass spectroscopy (MS), thermogravimetric analysis (TGA) and differential scanning calorimetry (DSC). The single crystal X-ray analysis showed that **T3** crystallizes in the monoclinic $P2_1/m$ space group with good reliability factor and that its crystal structure is organized by an alternation of hexachlorotellurate octahedral polyhedra $\{TeCl_6\}$ and benzimidazolium planes $\{C_7H_7N_2\}$ joined together through hydrogen bonds that ensure the cohesion and the overall stability. Exhaustive vibrational and optical studies of **T3** were performed through infrared absorption at room temperature and UV–vis spectroscopies, respectively. In the ultraviolet area **T3** has three absorption signals corresponding to charge transfers in the organic part, between the organic and inorganic moieties, and in the inorganic complex, as computationally confirmed. Theoretical calculations also reveal a HOMO-LUMO gap of 3.95 eV, large enough as to indicate stability against intramolecular electron excitation. Thermogravimetric data of the thermal decomposition of **T3** were also analysed revealing that the weight loss occurs in three stages. An isoconversional method was used for computing the activation energy and its variation along the thermal decomposition. Finally, and as a main feature of **T3**, antibacterial activity against *Escherichia coli* and *Staphylococcus aureus* stains has been tested and confirmed after incubation for 24 h at 37 °C of **T3** diluted at different concentrations (0.5–2 mg/ml) in ethanol or dimethyl sulfoxide (DMSO).

1. Introduction

Current times have seen a real explosion of new materials for chemistry and the industrial world. Many of them can be classified as Metal–Organic Frameworks (MOFs) [1,2], Covalent–Organic Frameworks (COFs) [3,4] and hybrid materials [5–7] and present applications in fields such as pharmaceutical, medical, biological [8–10], photocatalytic [11], catalytic [12], opto-electronics [13], sensing [14–16] and proton conductivity areas [17–19], among others. Particularly, hybrid materials are gaining attention in research because of their simple synthesis, adjustable structure and adaptive functionality. Usually, they integrate features of both organic and inorganic parts ensuring not only

the alloy of their individual properties but also giving rise to new characteristics resulting from the cooperation of the two species. Besides, one of them (organic or inorganic) usually has a nanometer size. Among all possible inorganic moieties available to build a hybrid material, tellurium complexes provide relevant properties. Tellurium is a rare metalloid with both metallic and non-metallic features which shows variable positive oxidation states of + 2, +4 and + 6. It is, however, a highly electronegative element able to combine to many aliphatic and cyclic organic compounds. The literature reports the synthesis and the investigation of relevant organo-tellurium compounds, [20–24] significant in chemistry, biology, medicine and, especially, the electronics industry [25–28]. To date, a specific grade is exclusively studied for

organic–inorganic hybrid compounds based on hexahalogentellurium, which shows copious structural arrangements in a notable number of elaborated compounds. The (4 +) oxidation state of tellurium has great interest in these hybrid compounds due to the Te octahedral coordination with halogens TeX_6 (with X = F, Cl, Br, I) [29–35].

Concerning the organic part, many hybrid materials have been developed based on the use of an amine generally protonated. Actually, this protonation plays an important role in several applications such as optics and catalysis [36–38]. Amine organic cations interact with anionic octahedral metal complexes through hydrogen bonds yielding structures with attractive chemical reactivity and physical properties [29,31–33,39–41]. In the large family of amines, countless reports have been posted on the benzimidazole one in sight of its broad ranging activities. Indeed, the use of $(C_7H_6N_2)$ and its derivatives appears not only in environmental, pharmaceutical, therapeutic, and medicinal [42–45], applications but also in chemical technology [46]. This benzimidazole cation has already been incorporated into the synthesis of hybrid compounds with important optical and microbiological responses [47–49].

Herein, as a contribution to the wide world of hybrid materials and as a part of our ongoing research collected in previous reports [50–53], the study of a new hybrid material incorporating hexachlorotellurate as the inorganic moiety and benzimidazole as the organic one, is performed. It leads to a novel compound, formulated as $(C_7H_7N_2)_2TeCl_6.(H_2O)_2$ (**T3**) that is stabilized by hydrogen bonds. (The **T3** name has been chosen taking into account other related hybrid materials under study in our group). Intermolecular interactions and bonds of **T3** are characterized by single crystal X-ray diffraction (SC-XRD), molecular weight quantifications, vibrational spectroscopy using Fourier-transform infrared (FT-IR) and UV–vis spectroscopies. Some experimental results are supported theoretical DFT calculations, which confirm the strong interactions between constitutive moieties and the perfect stability of the material. Besides, the antibacterial activity of **T3** is studied. As a whole, this research leads to the discovery of the physico-chemical, optical and biological properties of the title compound.

2. Experimental measurements

2.1. Chemical preparation

In the synthesis of **T3** all reagents are directly used without further purification. In a stoichiometric ratio, the tellurium dioxide TeO_2 (1.5 mmol) dissolved in 3 ml of a concentrated HCl (40 %) was stirred to obtained hexachlorotellurate molecules. The mixture was added to a solution of benzimidazole $C_7H_6N_2$ (2 mmol) in the presence of 7 ml of ethanol. Schematically the reaction is:

$$2\,C_7H_6N_2 + TeO_2 + 6\,HCl \rightarrow (C_7H_7N_2)_2TeCl_6.(H_2O)_2$$
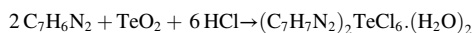
After stirring for 30 min, the achieved solution was subjected to slow evaporation at room temperature. Five days later, single crystals with clear contours were acquired, which were appropriate for the structural study.

2.2. Investigation methods

2.2.1. Micrographs and X-ray microanalysis
Scanning Electron Microscope (SEM) and Energy Dispersion X-ray Spectroscopy (EDXS) were recorded using a 30 kV JEOL-6610LV electron microscope attached to an Oxford X-Max Microanalysis System.

2.2.2. Single-crystal diffraction data collection and structure determination
A perfectly-formed single crystal of the obtained compound was cautiously selected for indexing under a microscope and mounted on a Mitegen micromesh mount with the help of a trace of mineral oil. Whole reflection intensity data were collected at room temperature on a Kappa CCD area-detector diffractometer [54] using the ω scan technique and furnished with CuKα (λ = 1.5406 Å) radiation. Using spherical

harmonics, empirical absorption corrections of the multi-scan type based on symmetry equivalents were applied. The space group was automatically search with WinGX [55]. The structure resolution was ensured by direct methods with the SHELXS97, olex2-1.2 programs [56,57] and completed by difference Fourier syntheses. Refinement was performed using the least squares fitting of complete matrix on F2 with the SHELXTL-2016 crystallographic software package including atomic coordinates and anisotropic thermal parameters for all non-hydrogen atoms. Geometrically calculated positions were attributed to hydrogen atoms of ligands and subsequently refined with fixed isotropic displacement parameters. The formula of the new compound (CCDC n°2128280) was purposed by chemical analysis and demonstrated by the complexion of the crystal structure. The projection of this structure in different planes was made using a Diamond program [58].

2.2.3. X-ray powder diffraction
Powder X-ray diffraction was recorded using the Cu-Kα radiation (1.5406 Å) with a 2θ range of 5–50° on a Siemens D5000 powder diffractometer in order to verify the purity of the synthesized material.

2.2.4. Infrared spectroscopy and UV–vis measurements
Spectroscopic study by infrared absorption at room temperature was performed with a ''Perkine–Elmer FTIR'' spectrophotometer 1000 using samples dispersed in spectroscopically pure KBr pellets functioning in the range 430–4000 cm^{-1}. Chemical analysis and IR spectrum were used in order to determine the functional groups present in the material and to confirm the formation of a new synthesized hybrid compound. The UV–visible absorption spectrum was registered in the 200–800 nm range using a Perkin Elmer Lambda 11UV/ Vis spectrophotometer at room temperature.

2.2.5. Mass spectrometry
A liquid chromatograph Agilent 1290 series (AgilentTechnologies, Santa Clara, CA) coupled to a triple quadrupole mass spectrometer Agilent 6460 equipped with an electrospray interface(ESI) with jet stream operating in positive ion mode was employedfor the analysis of the samples. The sample was disolved in a 1:1 mixture of water and Methanol with 0.1 % of formic acid. The analysis of the sample was carried out injecting 20 μl. Mobile phases A and B were water and methanol, both with 0.1 % formic acid and and the analysis was carried out in isocoratic mode at 50 % of mobile phase B. The ionisation source working conditionswere 5000 V as capillary voltage, 45 psi as nebuliser pressure, 11 $Lmin^{-1}$ as drying gas flow rate and 320∘C as drying gas temperature. The sheath gas flow rate and temperature were 12 L min^{-1} and 200∘C, respectively.

2.2.6. Theoretical calculations
To perform the theoretical analysis, we selected a neutral moiety of the crystal (made with two benzimidazolium cations, one $TeCl_6$ anion and two water molecules) having the strongest hydrogen bonds between the organic and inorganic fragments of our new hybrid material. The geometry and energy of this representative model was optimized without any constraints in ethanol solution with the Polarizable Continuum Model (PCM) [59–61] in conjunction with the hybrid density functional B3LYP [62–64] and the 6–31 + G(d) basis set for nonmetal atoms [65], together with the valence double-ζ basis set LANL2DZ plus the effective core potential of Hay and Wadt for the Te and Cl atoms [66], and by using a modified Schlegel [67–69] algorithm.

For interpretation purposes a natural orbital (NBO) analysis [70,71] was performed. It allowed the quantification of the atomic charges assigned to each atom and, particularly, to those involved in H bonds.

The UV–vis absorption spectra of **T3** was computed using the optimized geometries and applying the time-dependent DFT methodology (TD-DFT) [72,73] in ethanol solution. In order to visualize the charge transfer associated to the most significant UV–vis transitions in a compact way, their Natural Transition Orbitals (NTO) [74] were
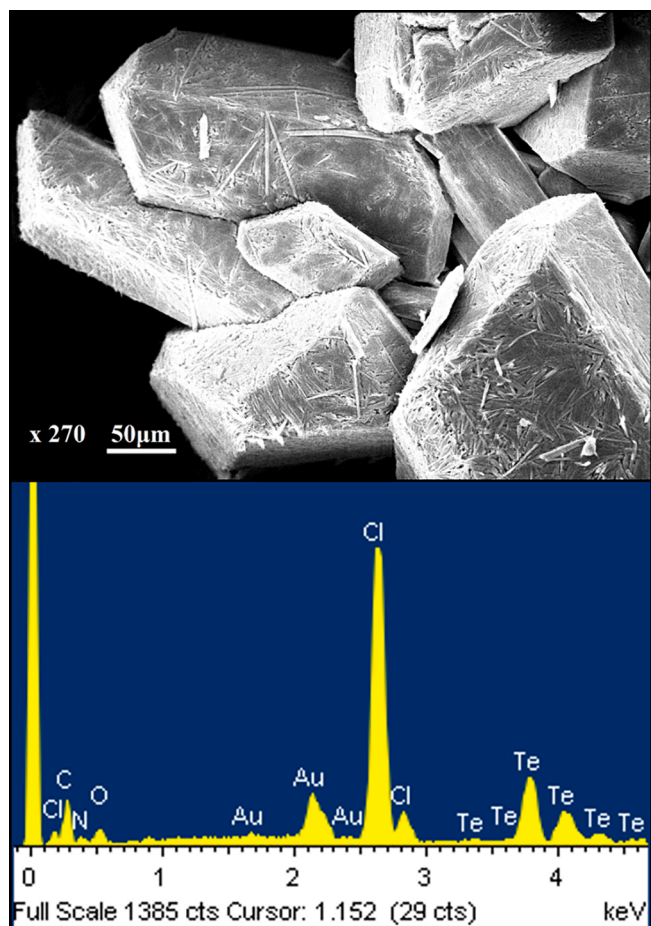
Fig. 1. Crystal morphology; scanning electron microscopy and typical EDX spectrum of **T3** sample.

calculated.

2.2.7. Thermal decomposition and its kinetics analysis

Thermogravimetric curves and differential thermal analyses were conducted by heating the powdered sample in an aluminum capsule using a TGA Q500 TA instrument. The scan was performed in flowing oxygen gas at a temperature range from 300 to 1000 K with a ramp rate of 10 K min^{-1}.

The differential scanning calorimetric (DSC) measurements were acquired with the SETARAM DSC131 ks instrument using a mass of 2.175 mg of **T3**, which was heated between 300 and 600 K at a rate of 10 K min^{-1} in air.

Our kinetics study provides information about the mechanism of the chemical decomposition of the sample during the heating. The reaction progress is given by the extent of conversion, $\alpha(t) = (m_0 - m(t))/(m_0 - m_f)$ where $m(t)$ is the mass at time t, and m_0 and m_f are the initial and final masses, respectively. The reaction rate of the process as a function of temperature is commonly described by the equation:

$$\frac{d\alpha}{dT}\beta = A\exp\left(-\frac{E}{RT}\right)f(\alpha)$$

where β is the heating rate, $f(\alpha)$ the reaction model, T (K) the temperature, A (s^{-1}) the pre-exponential factor, E (J/mol) the activation energy, and R (J/mol K^{-1}) the gas constant [75].

2.2.8. Biological activity

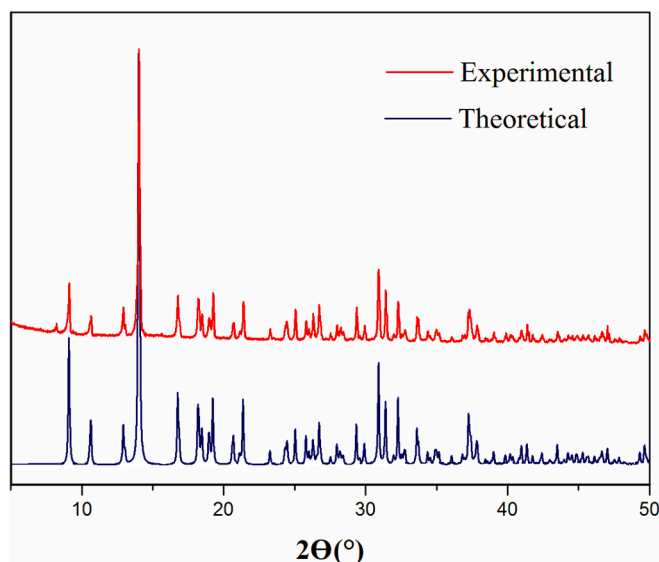Advanced biological and medical research on tellurium has

Fig. 2. Theoretical and experimental diffractograms of the **T3** powder.

concluded that compounds based on tellurium show significant antibacterial activities [76,77]. In order to assess these properties, the synthesized hexachlorotellurate hybrid material was examined against both gram-negative and gram-positive strain bacteria by Agar well diffusion techniques [78]. The bacteria used to test the antibacterial activity were *Staphylococcus aureus* (abbreviated as *Staph*) and *Escherichia coli* (abbreviated as *E. coli*). A fresh cell suspension of bacteria was speared onto the nutrient agar medium uniformly spread on the Petri dish plate. Using the sterile Pasteur pipettes, wells of 5 mm diameter were punctured in the center of the sectioned areas in the agar medium. To examine the efficacy of our new hybrid nanomaterial, 1 ml of the crystal sample, soluble in ethanol or dimethyl sulfoxide (DMSO), was placed in each well at different concentrations (0.5–2 mg/ml). The plate was incubated at 37 Celsius degrees under aerobic conditions to permit

Table 1

Main crystallographic features of X-ray diffraction data of **T3** structure.

Formula	$(C_7H_7N_2)_2TeCl_6.(H_2O)_2$
Formula weight	632.64
Temperature/K	293
Crystal or powder type	Yellow
Crystal size/mm	$0.311 \times 0.075 \times 0.059$
Crystal system	Monoclinic
Space group	$P2_1/m$
a/Å	7.2769(2)
b/Å	16.6286(3)
c/Å	10.3227(2)
α/°	90
β/°	109.719
γ/°	90
Volume/Å^3	1175.85(5)
Z, $\rho_{calculated}$/g cm^{-3}	2, 1.787
μ/mm^{-1}	16.467
Θ range/°	4.51–74.033
Limiting indices	$-12 \leq h \leq 12$
	$-17 \leq k \leq 17$
	$-19 \leq l \leq 19$
Collected reflections	2529
Observed reflections I > 2σ(I)	1853
Refined Parameters	143
Highest peak/deepest hole(eÅ^3)	$1.439 > \Delta\rho > -1.016$
R [F^2 > 2σ(F^2)]	0.0546
WR(F^2)	0.1772
GooF	1.1380
CCDC n°	2,128,280

WR = $(\sum[w(F^2_o - F^2_c)^2]/[w(F^2_o)^2])^{1/2}$ et R = $\sum||F_o| - |F_c||/\sum|F_o|$ GooF = S = $\{[w (F^2-F^2)^2] / (n-p)\} 1/2$.
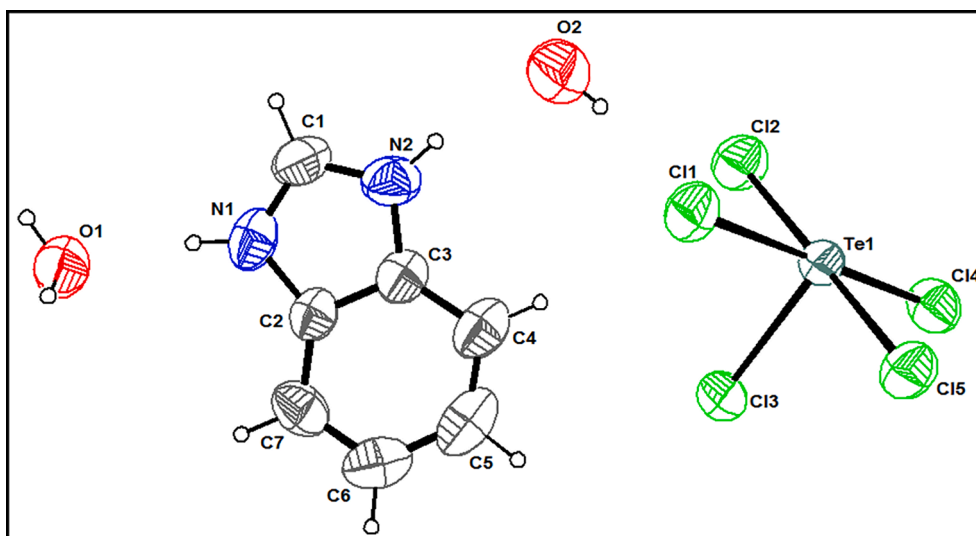
Fig. 3. The asymmetric unit with atom labels and 50% probability displacement ellipsoids for non-H atoms of **T3**.
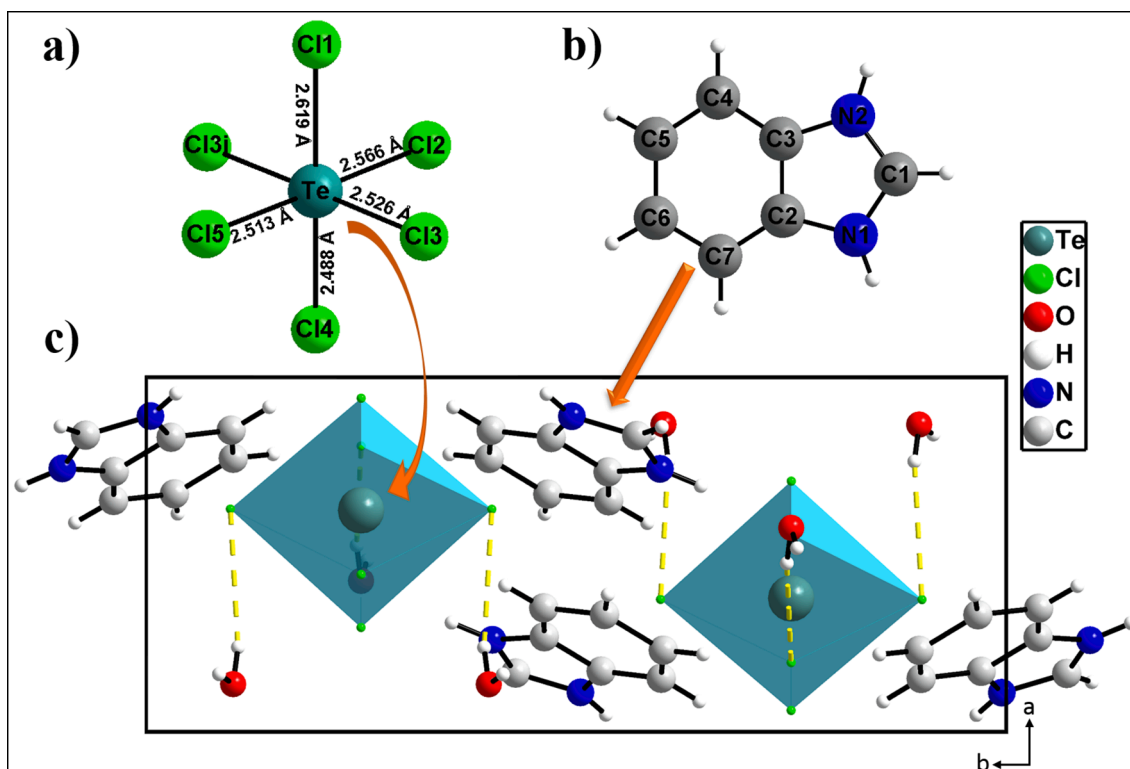

Fig. 4. a) Environment of tellurium complex b) Organic moiety c) Projection of **T3** crystal structure showing hydrogen bonds on the (ab) plane.

the diffusion of the hybrid compound and standards onto agar. After 24 h, a measurement of the inhibition zone diameters (IZD) gave access to the evaluation of antibacterial activity.

3. Results and discussion

3.1. Description of the structure

The views of the particle size and surface morphology of the powder, presented in Fig. 1, show a regular distribution of grains with some particle agglomerations. This indicates a good crystal quality

with flat surface. The results of this qualitative analysis confirm the presence of all non-hydrogen atoms expected during the preparation such as carbon, nitrogen, oxygen, chlorine and tellurium. The PXRD pattern of the compound was compared with the theoretical one (Fig. 2), illustrating that **T3** has been successfully obtained as a pure crystalline phase. The crystalline structure was elucidated by single crystal X-ray diffraction study. After the determination of the cell (indexing (h k l)) all the data obtained were recorded. According to the automated search for space group available in WinGX [55], the structure is solved in a monoclinic space group. Once the space group is known, treatment and refinement are done until the structure

Table 2
Interatomic distances and bond angles of **T3**.

Tellurium complex

Te(1)−Cl(4)=2.488(3)	Cl(4)−Te(1)−Cl(5)=90.30(11)
Te(1)−Cl(5)=2.513(3)	Cl(4)−Te(1)−Cl(3)=89.52(5)
Te(1)−Cl(3)=2.527(2)	Cl(5)−Te(1)−Cl(3)=90.15(5)
Te(1)−Cl(3i)=2.527(2)	Cl(4)−Te(1)−Cl(3i)=89.52(5)
Te(1)−Cl(2)=2.566(3)	Cl(5)−Te(1)−Cl(3i)=90.15(5)
Te(1)−Cl(1)=2.519(3)	Cl(3)−Te(1)−Cl(3i)=178.99(12)
	Cl(4)−Te(1)−Cl(2)=90.34(12)
	Cl(5)−Te(1)−Cl(2)=179.36(11)
	Cl(3)−Te(1)−Cl(2)=89.85(5)
	Cl(3i)−Te(1)−Cl(2)=89.85(5)
	Cl(4)−Te(1)−Cl(1)=179.31(11)
	Cl(5)−Te(1)−Cl(1)=90.39(11) Cl (3)−Te(1)−Cl(1)=90.48(5)
	Cl(3i)−Te(1)−Cl(1)=90.48(5) Cl (2)−Te(1)−Cl(1)=88.97(11)

Organic moiety

N1−C1=1.325(11)	C7−C2−N1=133.4(9)
N1−C2=1.385(10)	C4−C3−N2=129.7(9)
N2−C1=1.317(12)	N1−C2−C3=105.2(8)
N2−C3=1.384(11)	N2−C3−C2=106.9(7)
	C1−N2−C3=108.9(8)
C2−C7=1.368(12)	C1−N1−C2=109.7(7)
C2−C3=1.389(12)	N2−C1−N1= 109.2(8)
C3−C4=1.378(12)	C7−C2−C3=121.5(8)
C7−C6=1.366(13)	C7−C6−C5=120.0(9)
C4−C5=1.368(15)	C4−C5−C6=123.3(9)
C6−C5=1.426(16)	C5−C4−C3=114.4(10)
	C4−C3−C2=123.4(9)
	C6−C7−C2=117.4(9)

Symmetry codes: (i) + x, 3/2-y, +z.

Table 3
Hydrogen-bond and short contact geometry (Å, °).

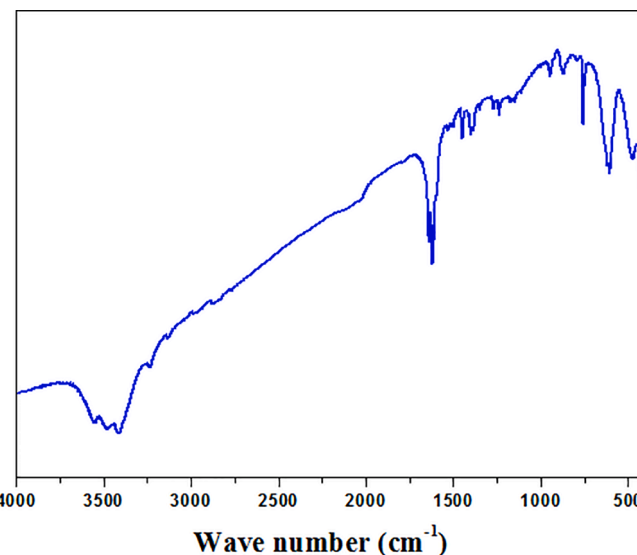| D–H...A	D–H	H...A	D...A	D–H...A
O2–H3···N2(ii)	0.83	2.55	2.882(11)	105.41
N1–H6···O1	0.86	2.02	2.674(11)	132.52
O2–H4···Cl2	0.84	2.71	3.403(14)	141
N2–H7···O2(iii)	0.86	2.04	2.882(11)	166.57

Symmetry codes: (ii) 1-x,-y, 1-z; (iii) 1-x, −1/2 + y, 1-z.

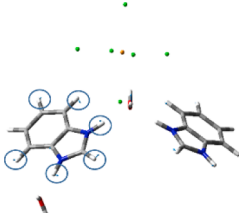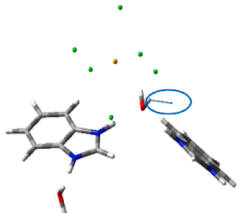**Fig. 5.** FT-Infrared spectra of **T3** at room temperature in N_2.

resolution and a structural model of the compound are achieved. The main crystallographic features of the X-ray diffraction results are summarized in Table 1. According to this basic information, **T3** crystallizes in the monoclinic system and solves in $P2_1/m$ space group with two formula units (Z = 2) at 293 K, cell parameters of $a = 7.2769(2)$ Å, $b = 16.6286(3)$ Å, $c = 10.3227(2)$ Å, $\beta = 109.719°$, and a volume of 1175.85(5) Å^3. The asymmetric formula unit is made up of one organic benzimidazole cation, one tellurium cation, five chloride anions and two water molecules (Fig. 3). The projection on the *ab* plane shows the coexistence of $(C_7H_7N_2)^+$ cations, $(TeCl_6)^{2-}$ anions and H_2O molecules in the unit cell. The structure arrangement on the [1 1 0] direction illustrates that the crystal structure is formed by water molecules and organic chains of $C_7H_7N_2$ situated at x/b = 0 and x/b= ½ between octahedral planes of $TeCl_6$ at x/b= ¼ and x/b= ¾ also stabilized by hydrogen bonds, which ensures the cohesion of these entities (Fig. 4.c)).

3.1.1. Geometry and environment of the inorganic component

The inorganic part of the title structure is composed of tellurium (IV) cations surrounded by six chloride ligands and occupies a special position in the material net (Fig. 4.a). This fact leads to the presence of just one type of octahedrons $TeCl_6$ with Te–Cl bond lengths ranging between 2.488(3) and 2.566(3) Å, and Cl–Te–Cl angles in the 88.97(11)-179.31(11)° range, (Table 2). These values agree with those of the $TeCl_6$ group in the (C3H8N6)2TeCl6.2Cl·(H2O)4 compound previously reported [79] since for this last material the Te–Cl distances are between 2.4785 (19) Å and 2.5542 (19) Å, while the Cl–Te–Cl angles vary in the range 88.01(6)-178.25(7)°.

3.1.2. Geometry and environment of the organic component

In the main part of the organic moieties, the two nitrogen atoms of the benzimidazole rings are mono-protonated (Fig. 4.b)), which allows the balancing the two excess negative charges carried by the inorganic part. These cations are mounted in a zero-dimensional arrangement by forming alternating layers with inorganic polyhedra as shown in Fig. 4. c). The $(C_7H_7N_2)$ group is characterized by interatomic N—C distances
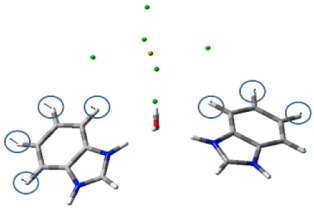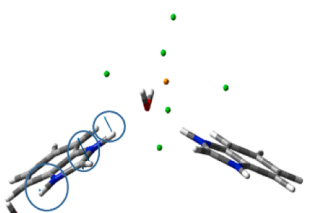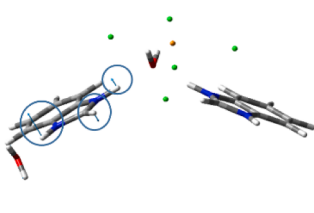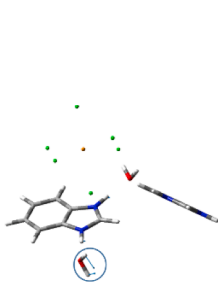
between 1.317(12) and 1.385(10) Å with C—C—N and C—N—C angles varying from 105.2(8) to 133.4(9)° and from 108.9(8) to 109.7(7)°, respectively. Besides, N—H bond distances are restricted to 0.89 Å for planar NR_2H groups, where N is sp2 hybridized, and C—H bond distances to 0.93 and 0.97 Å. The values of the distances and angles of the bonds characterizing the geometry of the organic cation are collected in the Table 2.

3.1.3. The hydrogen bonds

The cohesion and the interconnectivity between organic and inorganic species are mainly achieved thanks to the hydrogen bonds showed on Fig. 4.c). The projection along the *ac* plane shows that there are two different types of crystallized water molecules. One of them bonds to two organic entities through week interactions forming O—H···N angles around 105.41° and is in touch with a near chlorine atom of an octahedral complex. The Cl···H bond lengths vary from 1.514 to 2.939 Å forming O—H···Cl angles at about 141°. As it can be seen in the projection of structure (Fig. 4 c)), the remaining hydrogen atom of the azole group in the organic species interacts with the second class of water molecules via N—H···O hydrogen bonds yielding bond distances close to 2.02 Å and bond angles between 132.52 and 166.57°. The geometric characteristics of these low-energy interactions are displayed in Table 3.
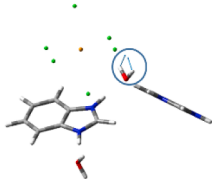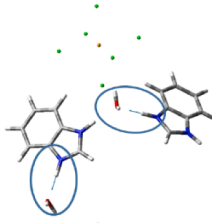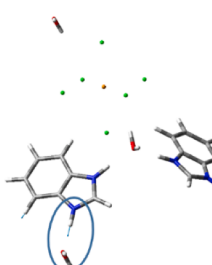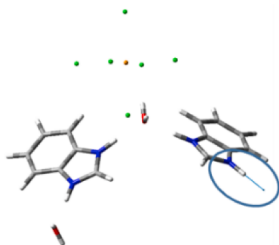
Comparing these values with analogous ones of similar hybrid materials reported in the literature, it can be said that hydrogen bonds in **T3** are regular. Indeed, in the previously reported hybrid material (C3H8N6)2TeCl6.2Cl·(H2O)4 [79], the N—H···O angles vary between 152.20 and 174.36° while the angles O—H···Cl and O—H···N equal to 163.98° and 167.25°, respectively [79]. The differences between H-bonds in this material and ours are expected due to their differences in the organic part and the number of water molecules present in each structure. Add-on, in the previously reported material a free chloride crystallizes, which does not happen in our crystal.

Table 4

Fourier Transform InfraRed frequencies (cm^{-1}) and band assignments of **T3**.

Assignment	IR Wave numbers (cm^{-1})	Calculated IR Wave numbers (cm^{-1})	Transition vectors of the most relevant calculated vibrations
δ (CCC); τ (C—N)	473	432.38	
δ (CCN)	475		
δ (CCN); δ (CNC)	606		
τ (H$_2$O)	620	515.20	
δ (C–H); ω (N—H)	758		
δ (C–H); υ (C—C); γ (OH)	871		
δ (CH)	946	766.30	
υ (C—C)	1112		
υ (C—N); υ (CC)	1149–1172	859.12	
		989.57	
υ (C—N)	1238		
δ (N—H)	1270		
δ (C—H)	1346		
υ (OH)	1383		
β (C–H)	1399		
δ (NH)	1451		
υ (C—N)	1503		
υ (CC)	1532		
(H$_2$O) deformation	1618	1666.40	

Table 4 (*continued*)

Assignment	IR Wave numbers (cm^{-1})	Calculated IR Wave numbers (cm^{-1})	Transition vectors of the most relevant calculated vibrations
		1686.55	
υ (CC); δ (C—H); β(N—H)	1638		
υ$_{as}$ (CH)	2770		
	2874		
	2966		
υ (C—H); υ (N—H)	2986		
υ (CH)	3132		
υ$_s$ (N—H)	3233	3209.50	
		3220.18	
		3220.61	
υ$_s$ (H$_2$O)	3412		
υ$_{as}$ (N—H)	3479	3631.11	
υ (C—H)	3553		

υ: stretching; **δ**: scissoring; **τ**: torsion; **ρ**: rocking; **ω**: wagging, **as**: asymmetric, **s**: symmetric, **β**: in-plane bending.

3.2. Infrared spectroscopy

In order to identify the specific functional groups, present in the title compound, infrared spectroscopy analysis was performed. The vibrational spectrum, measured at room temperature between 400 and 4000 cm^{-1}, is shown in Fig. 5. Thorough assignments of the observed bands were made based on a comparison with experimental results reported in the literature for similar compounds [39,50–52,79–85], on visual scrutiny of the wavenumbers, and on the calculated IR spectrum. The experimental assignments are collected in the Table 4 along with the calculated displacement vectors associated to the most relevant normal vibrational modes. Some calculated IR peaks appear somehow displaced in comparison with experimental ones, but, once related to the corresponding experimental absorption, may give light in the description of

the associated vibrational mode.

At the high IR frequency domain, the symmetric and asymmetric stretching of N—H bonds appear at 3233 and 3479 cm^{-1} [80]. The peaks at 1270, 1451 and 2986 cm^{-1} are assigned to the scissoring and stretching of the (NH) groups [50,52]. Furthermore, peaks at 2770–3132 and 3553 cm^{-1} correspond to the stretching wave number of (C—H) [51,79,81,82]. However, the vibration modes situated at 1346 and 1399 cm^{-1} are attributed, respectively, to the β (C—H) and scissoring modes of (CH) groups [52,79]. Meanwhile, the peak observed at 1238 cm^{-1} and 1638 cm^{-1} was ascribed to the υ (C—N), υ (CC), δ (C—H) and β (N—H) vibration modes [50,81]. Absorptions detected at 1149–1172, 1503 and 1532 cm^{-1} can be attributed to the υ (CC), υ (C—N) vibrations in the organic moiety [81,83,84]. Besides, absorptions in the 758–1112 cm^{-1} region correspond to the ω (N—H), υ (C—C) and δ (C—H)
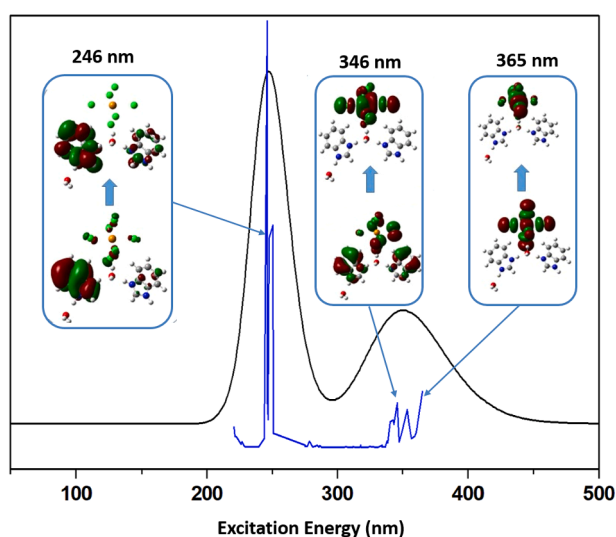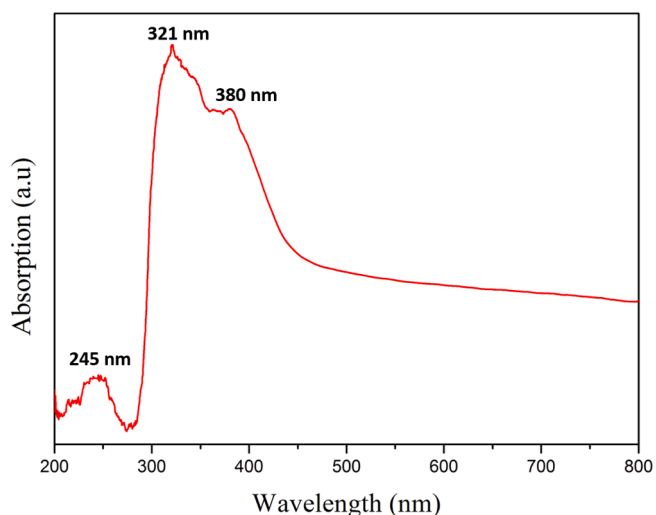
Fig. 6. UV–Visible absorption spectra top) experimental, below) theoretical for **T3** at room temperature.

vibrations [51,80–84].

Finally, the IR spectrum shows at low frequency, in the 473–606 cm^{-1} range, a set of peaks and bands which are probably the result of scissoring δ (CCC), δ (CCN), δ (CNC) and torsion τ (C—N) vibrations of the organic motif [80,82,84].

The presence of water molecules in **T3** is suggested by the vibration bands observed at 620 and 3412 cm^{-1} related, respectively, to symmetric stretching and torsion of H_2O [83,84]. Peaks detected at 1618 cm^{-1} correspond to the deformation mode of this group [85]. Also, the scissoring and stretching modes of the OH groups are observed at 871 and 1383 cm^{-1}, respectively [81].

According to prior IR spectra of halogenotellurate hybrid materials, the internal vibrational modes of similar inorganic entities appear below 400 cm^{-1}, [39,79] so they cannot be seen in the range here considered.

3.3. UV–vis absorption

The UV–visible absorption spectrum of **T3** was explored in range from 200 to 800 nm at room temperature (Fig. 6), and exhibits a notable absorption in the ultraviolet range at 245, 321 and 380 nm. According to numerous studies on materials belonging to the same family of hybrid compounds, the first peak detected at 245 nm (4.99 eV) can be due to the π-π* transitions of the benzimidazole rings [34,86–88]. The strongest peak at 321 nm (3.74 eV) can be assigned to ligand-to-metal charge transfer bands [79]. The third one at 380 nm (3.12 eV) may come from the electronic excitations between the excited state sp and the ground state s^2 of the telluric center: Te(IV) [39,79,89,90]. Essentially, large energy is needed to promote electrons to higher orbitals, since the crystalline structure absorbs light in the UV region.

Fig. 6 also displays the UV spectrum of **T3** computationally obtained. Some of the main bands experimentally detected appear with those around 321 nm a bit red-shifted and split. The intensity of theoretical bands is expressed relative to the most intense one, so it is not directly related to the intensity of experimental bands. The use of Natural Transition Orbitals (also depicted in Fig. 6) allows the overview of charge displacement associated to each band and nicely confirms the assignment done on basis of previous experimental studies, that is, the band at 246 nm corresponds to a π-π* transition at the benzimidazole ring and those at 365 and 346 nm are ligand-to-metal transition and excitations from the aromatic amine rings to the metal complex, respectively.
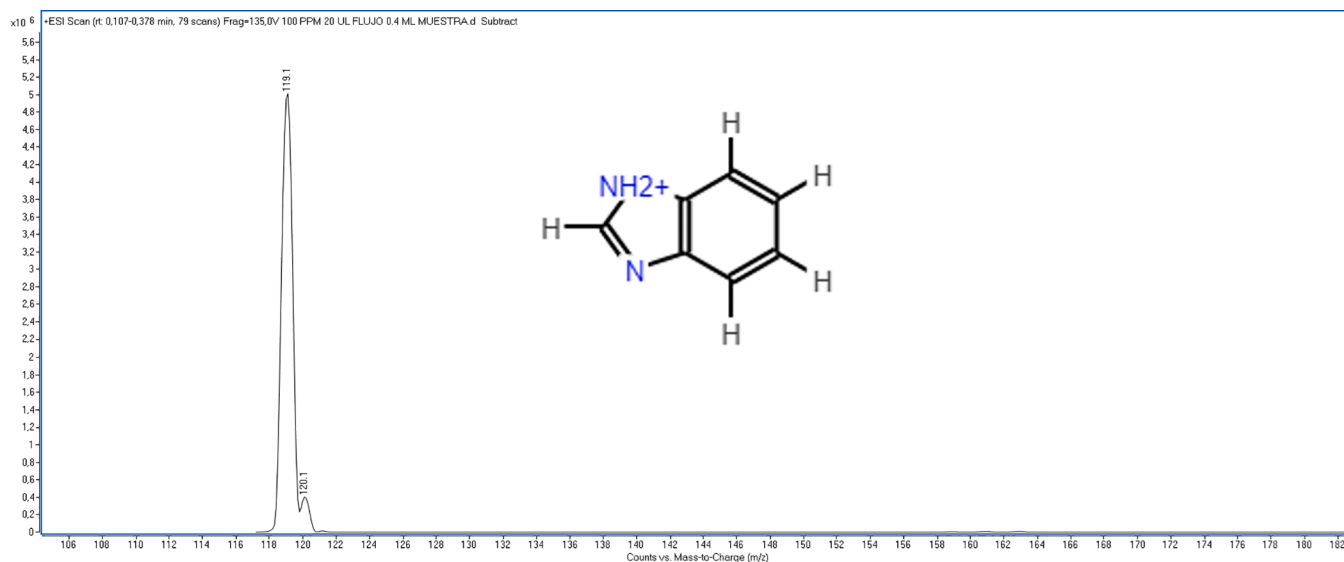

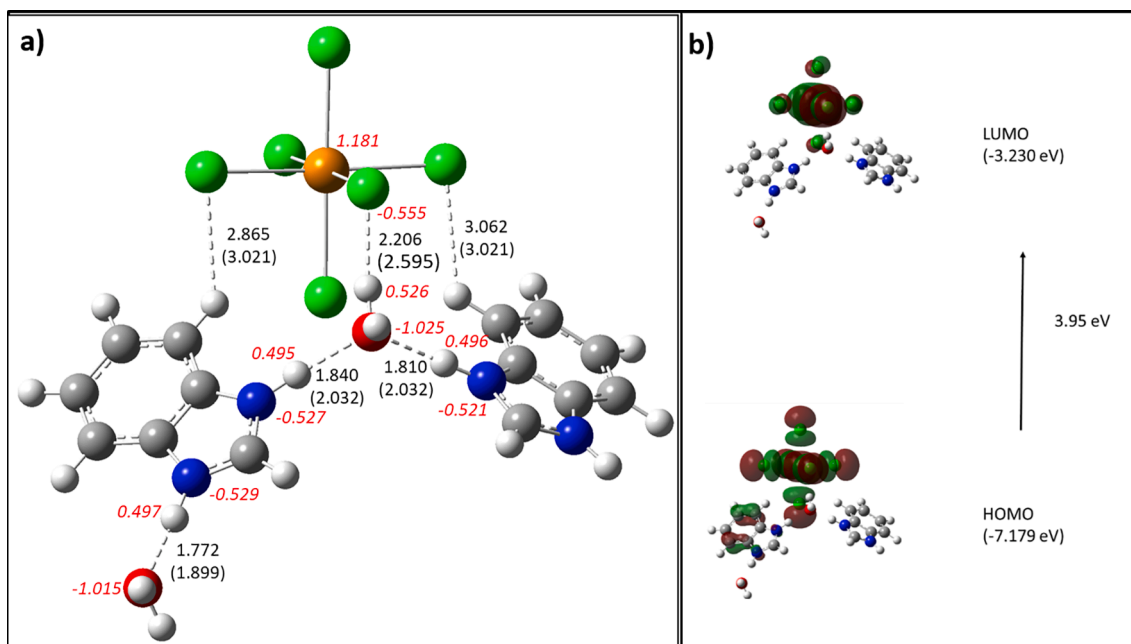**Fig. 7.** Mass spectroscopy spectra of **T3**.

Fig. 8. a) B3LYP/6-31+G(d) (LANL2DZ for Te and Cl atoms) bond distances optimized in ethanol solution (data in parenthesis come from X-ray data of the crystal sample) and NBO atomic charges in red. b) shape and energy of the frontier MO of the theoretically analysed moiety. (For interpretation of the references to colour in this figure legend, the reader is referred to the web version of this article.)
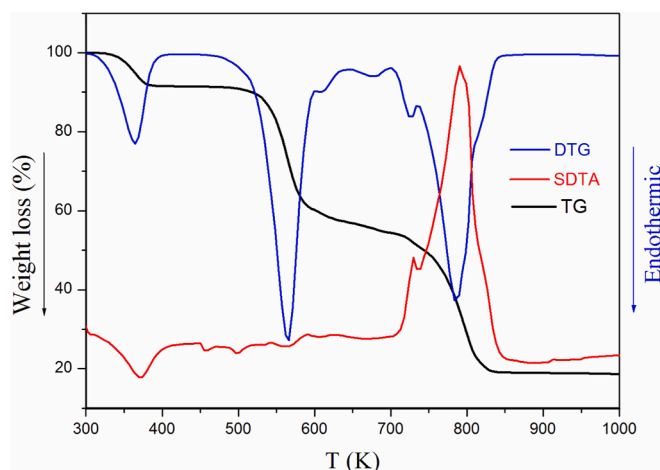

Fig. 9. Thermo-Gravimetric curve of **T3** at a ramp rat of 5 K min^{-1} in flowing oxygen gas.

3.4. Mass spectrometry analysis

The analysis was carried out in scan mode selecting a mass range from 100 to 1000 *m/z*. As can be oberved in the MS spectra (Fig. 7) a major intensity was found at *m/z* 119,1 which corresponds to the protonated [M + H] + ion being M: $C_7H_7N_2$ (benzimidazole moiety).

3.5. Computational results

As previously said, the structure selected as representative of the crystal is a neutral one made of two benzimidazolium cations, one $TeCl_6^{2-}$ complex and two water molecules. This model was chosen to include the strongest hydrogen bonds between the organic and inorganic fragments of the new hybrid material. The geometry of the representative model was optimized without any constraints in ethanol solution and Fig. 8.a shows how bond intermolecular distances closely resemble those provided by X-ray analysis. This fact supports the adequacy of the model
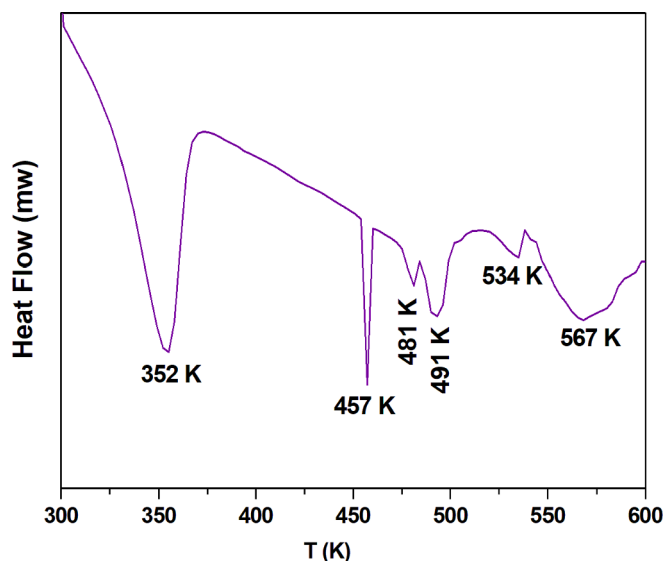

Fig. 10. DSC curve of the **T3** at a heating rate of 10 K min^{-1} in O_2 medium.

selected for the theoretical characterization of the new hybrid material (including the interpretation of IR and UV spectra just described).

Fig.8.a) also displays the NBO atomic charges of the atoms involved in the main H-bond network responsible of the stability of the material. It is clarifying to see how positively charged H atoms (with an average charge close to + 0.500 e) are shared by strong electronegative elements like N (average charge of −0.520 e), O (average charge of −1.020 e), and Cl (charge of −0.555 e) atoms.

The shape, orbital energy and energy gap between the HOMO and LUMO orbitals are displayed in Fig. 8.b). The HOMO orbital spreads over the $TeCl_6^{2-}$ complex and the benzyl ring of one of the organic molecules, whereas in LUMO one only involves the metal complex. There is a HOMO-LUMO gap of 3.95 eV that matches quite well with the UV transition involving the organic and the inorganic fragments (3.74 eV)
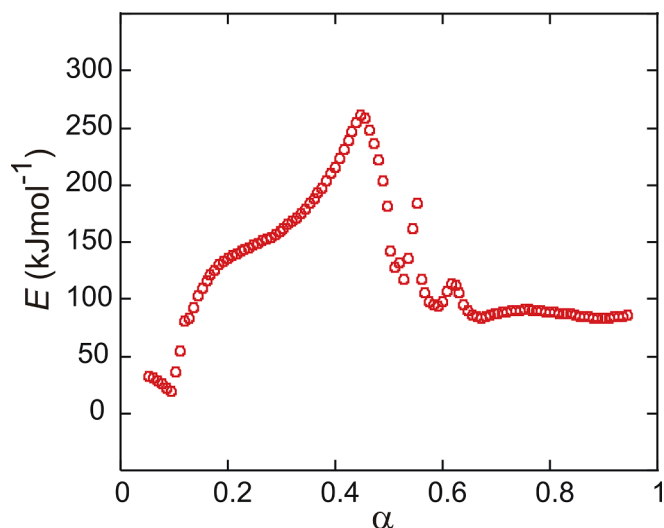
Fig. 11. Activation energy.

and suggests a large stability of the system against electron excitation.

3.6. Thermal decomposition

The thermal decomposition of **T3** under O_2 atmosphere proceeds through three stages recording to 81.89 % (calc. 80.74 %) of the total weight loss that can be observed on TG/DTG curves in Fig. 9. The first weight loss (obs. 8.52 %, calc. 8.64 %) is assigned to the release of two H_2O molecules and happens between 321 and 402 K. The endothermic peak at 363 K in SDTA (Fig. 8) and also the signal at T = 352 K ($\Delta H_1 = 269.75$ Jg^{-1}) in DSC curve confirm this dehydration (Fig. 10) [79,83,91,92].

Above 402 K, the anhydrous complex continues to decompose with 72.37 % loss of total mass on the TG curve (calc. 72.1 %). This transformation is related to a material decomposition that is verified by the successive endothermic peaks observed on DSC between 454 and 595 K with a total value of its enthalpy transitions equal to $\Delta H_2 = 164.38$ J. g^{-1}.

At the temperature 494 K, the second weight loss was triggered with the expulsion of chlorine in the form of HCl, which agrees with the endothermic intense peak in DTG curve at 565 K. This phenomenon

Table 5
Antibacterial activity of **T3**.

Bacteria		Staphylococcus	E. coli
Solvent	Concentration (mg/ml)	IZD (millimeter)	IZD (millimeter)
Ethanol	Control (Ethanol)	9.5	9
	0.5	15	12.5
	1	15	14.5
	1.5	15.5	13
	2	20	14
DMSO	Control (DMSO)	7	0
	0.5	0	22
	1	0	22.5
	1.5	0	12.5
	2	13.5	11

continues until the loss of two chlorine and the formation of tetrachlorotellurate.

Afterwards, the peak at 670 K in DTG corresponds to the release of $TeCl_4$ since the boiling point of $TeCl_4$ at atmospheric pressure is close to 663 K, which confirms the evaporation of $TeCl_4$ [79]. In addition, the tiny endothermic process around 725 K agrees with the melting point of pure tellurium (722.5 K) [79].

The third weight loss took place later as a result of the interaction of carbon and nitrogen with oxygen in the medium, asserted with intense peaks on SDTA/DTG around 790 K, which led to the total decomposition of the organic part as nitrogen dioxide and carbon dioxide gases. After several degradations, no thermal phenomenon was detected above 900 K and the final product obtained was a trace of tellurium equal to 18.13 % (Calc. 20.76 %).

The kinetics of the thermal decomposition was analysed assuming an oxygen atmosphere and considering three heating rates, $\beta = 5, 10$, and 15 K min^{-1}. The activation energy E was computed by using the modified version of the differential isoconversional Friedman method proposed in reference [93]. Fig. 11 shows the obtained results.

For the first weight loss, $\alpha \leq 0.1$, E decreases from 32.7 down to 19.2 kJ mol^{-1}. These low values of E agree with the easy release of water from the sample. At the second step, for $0.1 < \alpha \leq 0.59$, the activation energy shows abrupt changes due to the complex decompositions above described for this temperature range. The maximum value for the activation energy is 259.3 kJ mol^{-1} for $\alpha = 0.45$ and the minimum is 93.7 kJ mol^{-1}, for $\alpha = 0.59$. At the third step, for $0.59 < \alpha$, that corresponds to the total decomposition of the organic part, E has an average value of 88.1 kJ mol^{-1}. In order to check the obtained values, the effective pre-
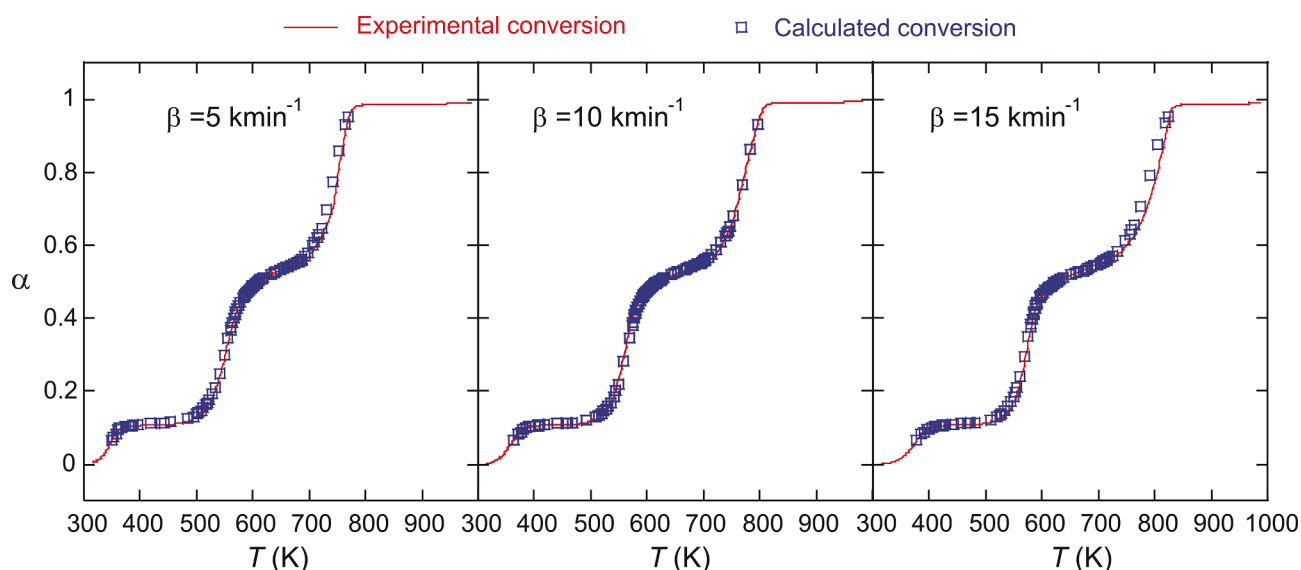

Fig. 12. Comparison of the reconstructed and experimental α-T curves.

factor c = Af(α) α-T curves were reconstructed showing a good agreement with the experimental ones (Fig. 12).

3.7. Biological activity of T3

The appraisal of the antibacterial power of our synthesized material against gram-negative (*E. coli*) and gram-positive (*Staph*) bacteria was studied using the simple and rapid technique of the agar diffusion assay. The antibacterial activity of **T3** was compared with that of the standards (ethanol and DMSO) and the mean diameters of inhibition zones (IZD) are summarized in Table 5.

T3 presents moderate activities on incubated bacteria. Indeed, the activity against *Staph* bacteria in ethanol raises as the concentration of **T3** increases from 0.5 to 2 mg/ml (IZD between 15 mm and 20 mm). Unlike in ethanol solution, **T3** diluted in DMSO presents relatively good activity against *Staph* only at a concentration equal to 2 mg/ml (IZD = 13.5 mm). The activity against *E. coli* shows a maximum of IZD at concentrations of 1 mg/ml, with IZD values equal to 14.5 mm and 22.5 mm, in ethanol and DMSO, respectively.

Based on the results obtained, it can be concluded that both the concentration of our hybrid compound and the solvent choice strongly influence its antibacterial activity. Furthermore, the presence of chlorine in the structure boosts its ability to inhibit the multiplication of *E. coli* and *Staph*, so it can be considered like a bacteriostatic substance. This antibacterial property makes **T3** more attractive compared to similar hybrid materials that showed a low reaction against these bacteria such as $(C_{12}H_{14}N_2O_2S)_2[Bi_4I_{16}]\cdot 4H_2O$ and $(C_{10}H_{28}N_4)[CoCl_4]_2$ [94,95].

Taking into account the properties of the new synthesized compound and those of similar ones collected in the literature, further research is needed to determine potential correlations between structure and biological activities of these materials.

4. Conclusions

In summary, a new $(C_7H_7N_2)_2TeCl_6\cdot(H_2O)_2$ hybrid material **T3** was prepared by the slow evaporation method at room temperature. The X-ray diffraction determined a molecular structure crystallizing in the monoclinic system with $P2_1/m$ space group. The crystalline structure is built up by $TeCl_6^{2-}$ octahedrons, $(C_7H_7N_2)^+$ organic cations and water molecules which contribute to the consolidation of the structure via O—H···Cl, O—H···N and N—H···O hydrogen bonds. The study of the vibrational properties of **T3** by infrared spectroscopy at room temperature allowed us to assign the different modes of vibration and confirm the nature of the units forming **T3**. The ultraviolet spectrum of **T3** has three absorption signals at 245, 321 and 380 nm as the main features of its optical behavior. Previous experimental studies on similar materials as well as theoretical calculations coincide in the assignation of the shortest wavelength band to charge transfer in the organic part (245 nm) and those at longer wavelengths to transitions between the organic and inorganic moieties, and inside the inorganic complex, respectively. The HOMO-LUMO gap theoretically calculated for **T3** is similar to that of related materials and corresponds to a chemically stable system against internal electronic excitations. The thermal decomposition occurs through three stages showing a dehydration followed by the decomposition of inorganic and organic structures with total loss of mass at approximately 79 %. The computed activation energies at different extents of degradation and the effective pre-factor provide a good description of the kinetics of the decomposition process. Furthermore, **T3** reveals *in vitro* quite favorable antibacterial properties and good inhibition zone diameters (IZD) against *Escherichia coli* and *Staphylococcus aureus* stains in different concentrations and solvents. Overall, a new solid hybrid material combining the characteristics of benzimidazole and tellurium hexachloride has been synthesized and carefully characterized. Its antibacterial properties provide it with potential applications in medical environments.

CRediT authorship contribution statement

Fatma Bentahar: Conceptualization, Methodology, Software, Investigation, Writing – original draft. **Mohammed S.M. Abdelbaky:** Conceptualization, Software, Investigation, Validation, Supervision, Writing – review & editing. **M. Isabel Menéndez:** Software, Investigation, Validation, Writing – review & editing. **Pedro Huidobro:** Software, Investigation, Validation, Writing – review & editing. **Santiago García-Granda:** Conceptualization, Supervision, Writing – review & editing. **Mohamed Dammak:** Conceptualization, Supervision, Writing – review & editing.

Declaration of Competing Interest

Data availability

The data that has been used is confidential.

Acknowledgment

Appendix A. Supplementary data

CDCC n°2128280 contains the supplementary crystallographic data for the compound **T3**. These data can be obtained free of charge at https://www.ccdc.cam.ac.uk or from the Cambridge Crystallographic Data Centre, 12 Union Road, Cambridge CB2 1EZ, UK; fax: (+44) 1223-336-033; or E-mail: deposit@ccdc.cam.ac.uk.

References

[1] X.J. Kong, T. He, Y.Z. Zhang, X.Q. Wu, S.N. Wang, M.M. Xu, G.R. Si, J.R. Li, J. Chem. Sci. 10 (2019) 3949–3955, https://doi.org/10.1039/c9sc00178f.
[2] G. Avci, I. Erucar, S. Keskin, J. Appl. Mater. Interfaces 12 (2020) 41567–41579, https://doi.org/10.1021/acsami.0c12330.
[3] X.T. Li, J. Zou, T.H. Wang, H.C. Ma, G.J. Chen, Y.B. Dong, J. Am. Chem. Soc. 142 (2020) 6521–6526, https://doi.org/10.1021/jacs.0c00969.
[4] F. Haase, B.V. Lotsch, J. R. Soc. Chem. 49 (2020) 8469–8500, https://doi.org/10.1039/d0cs01027h.
[5] I. Feddaoui, M.S.M. Abdelbaky, S. García-Granda, C. Ben Nasr, M.H. Mrad, J. Mol. Struct. 1211 (2020) 128056. doi: 10.1016/j.molstruc.2020.128056.
[6] L.T. López, D. Ramírez, F. Jaramillo, J.A. Calderón, J. Electrochim. Acta 357 (2020), 136882, https://doi.org/10.1016/j.electacta.2020.136882.
[7] R. Essalhi, M.S.M. Abdelbaky, S. Elleuch, F. Zouari, S. García-Granda, J. Mol. Struct. 1221 (2020), 128828, https://doi.org/10.1016/j.molstruc.2020.128828.
[8] W.J. Peveler, J.C. Bear, P. Southern, I.P. Parkin, J. Chem. Commun. 50 (2014) 14418–14420, https://doi.org/10.1039/C4CC05745G.
[9] I. Hamdi, I. Bkhairia, A. Roodt, T. Roisnel, M. Nasri, H. Naïli, J. R. Soc. Chem. 10 (2020) 5864–5873, https://doi.org/10.1039/c9ra09294c.
[10] E. Ruiz-Hitzky, P. Aranda, M. Darder, G. Rytwo, J. Mater. Chem. 20 (2010) 9306–9321, https://doi.org/10.1039/c0jm00432d.
[11] J. Wang, A.S. Cherevan, C. Hannecart, S. Naghdi, S.P. Nandan, T. Gupta, D. Eder, J. Appl. Catal. B: Environmental 283 (2021), 119626, https://doi.org/10.1016/j.apcatb.2020.119626.
[12] C. Sanchez, B. Julian, P. Belleville, M. Popall, J. Mater. Chem. 15 (2005) 3559–3592, https://doi.org/10.1039/b509097k.
[13] I. Matulková, J. Cihelka, M. Pojarová, K. Fejfarová, M. Dušek, P. Vaněk, J. Kroupa, R. Krupková, J. Fábry, I. Němec, J. Cryst. Eng. Comm. 14 (2012) 4625–4636, https://doi.org/10.1039/C2CE00024E.
[14] G. Lin, H. Ding, D. Yuan, B. Wang, C. Wang, J. Am. Chem. Soc. 138 (2016) 3302–3305, https://doi.org/10.1021/jacs.6b00652.
[15] Q. Hao, C. Zhao, B. Sun, C. Lu, J. Liu, M.J. Liu, L.J. Wan, D. Wang, J. Am. Chem. Soc. 140 (2018) 12152–12158, https://doi.org/10.1021/jacs.8b07120.

[16] L. Ascherl, E.W. Evans, M. Hennemann, D.D. Nuzzo, A.G. Hufnagel, M. Beetz, R. H. Friend, T. Clark, T. Bein, F. Auras, J. Nat. Commun. 9 (2018) 3802, https://doi. org/10.1038/s41467-018-06161-w.

[17] G.H.V. Bertrand, V.K. Michaelis, T.C. Ong, R.G. Griffin, M. Dincă, J. Proc. Natl. Acad. Sci. U. S. A. 110 (2013) 4923–4928, https://doi.org/10.1073/ pnas.1221824110.

[18] Y. Du, H. Yang, J.M. Whiteley, S. Wan, Y. Jin, S.H. Lee, W. Zhang, J. Angew. Chem. Int. Ed. 55 (2016) 1737–1741, https://doi.org/10.1002/anie.201509014.

[19] H. Li, J. Chang, S. Li, X. Guan, D. Li, C. Li, L. Tang, M. Xue, Y. Yan, V. Valtchev, S. Qiu, Q. Fang, J. Am. Chem. Soc. 141 (2019) 13324–13329, https://doi.org/ 10.1021/jacs.9b06908.

[20] A.Z. Al-Rubaie, N.I. Al-Salim, S.A.A. Al-Jadaan, J. Thermochim. Acta 215 (1993) 235–240, https://doi.org/10.1016/0040-6031(93)80097-T.

[21] A.Z. Al-Rubaie, A.K. Al-Derawi, J. Heteroat. Chem. 18 (2007) 93–99, https://doi. org/10.1080/00958972.2018.1478085.

[22] Y.J. Cui, F. Hu, A.Q. Jia, Z.F. Xin, Q.F. Zhang, J. Coord. Chem. 71 (2018) 1–11, https://doi.org/10.1080/00958972.2018.1478085.

[23] S. Mo, Z. Ju, Z. Xu, J. Wu, K. Yao, J. Inorg. Nano-Met. Chem. 36 (2006) 687–692, https://doi.org/10.1080/15533170600962554.

[24] R. Kaur, H.B. Singh, R.J. Butcher, J. Organomet. 14 (1995) 4755–4763, https:// doi.org/10.1021/om00010a043.

[25] R.L.O.R. Cunha, I.E. Gouvea, L. Juliano, J. An. Acad. Bras. Cienc. 81 (3) (2009) 393–407, https://doi.org/10.1590/s0001-37652009000300006.

[26] B. Sredni, J. Semin, Cancer Biol. 22 (2012) 60–69, https://doi.org/10.1016/j. semcancer.2011.12.003.

[27] T. Chivers, R.S. Laitinen, J. Chem. Soc. Rev. 44 (2015) 1725–1739, https://doi. org/10.1039/c4cs00434e.

[28] J. Ibers, Tellurium in a twist, J. Nat. Chem. 1 (2009) 508. doi: 10.1038/nchem.350.

[29] H. Kiriyama, Y. Mizuhashi, J. Ootani, J. Bull. Chem. Soc. Jpn. 59 (1986) 581–585, https://doi.org/10.1246/bcsj.59.581.

[30] H. Kiriyama, K. Nishizaki, J. Bull. Chem. Soc. Jpn. 59 (1986) 2415–2419, https:// doi.org/10.1246/bcsj.59.2415.

[31] M. Fizer, M. Slivka, R. Mariychuk, V. Baumer, V. Lendel, J. Mol. Struct. 1161 (2018) 226–236, https://doi.org/10.1016/j.molstruc.2018.02.054.

[32] M. Fizer, M. Slivka, V. Sidey, V. Baumer, O. Fizer, J. Mol. Struct. 1241 (2021), 130632, https://doi.org/10.1016/j.molstruc.2021.130632.

[33] M. Fizer, M. Slivka, V. Sidey, V. Baumer, R. Mariychuk, J. Mol. Struct. 1235 (2021), 130227, https://doi.org/10.1016/j.molstruc.2021.130227.

[34] M. Mhiri, M. Boujelbene, J. Polym. Bull. (2021), https://doi.org/10.1007/s00289-021-03758-y.

[35] M. Mhiri, O. Kammoun, J. Lhoste, S. Auguste, M. Boujelbene, J. Polym. Bull. (2022), https://doi.org/10.1007/s00289-021-04053-6.

[36] X.F. Zhu, D.Q. Shi, J. Heterocycl. Chem. 48 (2011) 572, https://doi.org/10.1002/ jhet.390.

[37] B. Moulton, M.J. Zaworotko, J. Chem. Rev. 101 (2001) 1629–1658, https://doi. org/10.1021/cr9900432.

[38] S. Kitagawa, R. Kitaura, S.I. Noro, J. Angew. Chem. Int. Ed. 43 (2004) 2334–2375, https://doi.org/10.1002/anie.200300610.

[39] D. Maraii, J. Farjas, X. Fontrodona, M. Dammak, J. Chin. Chem. Lett. 28 (2017) 1773–1779, https://doi.org/10.1016/j.cclet.2017.04.005.

[40] D. Maraii, M. Dammak, J. Mol. Struct. 1217 (2020), 128427, https://doi.org/ 10.1016/j.molstruc.2020.128427.

[41] M. Mhiri, O. Kammoun, J. Lhoste, S. Auguste, H. Ammar, M. Boujelbene, J. Mol. Struct. 1251 (2022), 131994, https://doi.org/10.1016/j.molstruc.2021.131994.

[42] M.S. Vasava, M.N. Bhoi, S.K. Rathwa, D.J. Jethava, P.T. Acharya, D.B. Patel, H. D. Patel, J. Mini Rev. Med. Chem. 20 (2020) 532–565, https://doi.org/10.2174/ 1389557519666191122125453.

[43] Y. Bansal, O. Silakari, J. Bioorg. Med. Chem. 20 (2012) 6208–6236, https://doi. org/10.1016/j.bmc.2012.09.013.

[44] S. Rajesekhar, B. Maiti, M.M. Balamurali, K. Chanda, J. Curr. Org. Synth. 14 (2017) 40–60, https://doi.org/10.2174/1570179413666160818151932.

[45] W. Akhtar, M.F. Khan, G. Verma, M. Shaquiquzzaman, M.A. Rizvi, S.H. Mehdi, M. Akhter, M.M. Alam, Eur. J. Med. Chem. 126 (2017) 705–753, https://doi.org/ 10.1016/j.ejmech.2016.12.010.

[46] E. Horak, P. Kassal, I.M. Steinberg, J. Supramol. Chem. 30 (2017) 838–857, https://doi.org/10.1080/10610278.2017.1403607.

[47] H.K. Gençer, U.A. Çevik, S. Levent, B.N. Sağlık, B. Korkut, Y. Özkay, S. Ilgın, Y. Öztürk, J. Molecules 22 (2017) 507, https://doi.org/10.3390/ molecules22040507.

[48] D. Mantu, V. Antoci, C. Moldoveanu, G. Zbancioc, I.I. Mangalagiu, J. Enzyme Inhib. Med. Chem. 31 (2016) 96–103, https://doi.org/10.1080/ 14756366.2016.1190711.

[49] A. Sharma, V. Luxami, K. Paul, J. Bioorg. Med. Chem. Lett. 23 (2013) 3288–3294, https://doi.org/10.1016/j.bmcl.2013.03.107.

[50] S. Bouketaya, M. Smida, M.S.M. Abdelbaky, M. Dammak, S. García-Granda, J. Solid State Chem. 262 (2018) 343, https://doi.org/10.1016/j.jssc.2018.03.039.

[51] S. Bouketaya, A. Elferjani, M.S.M. Abdelbaky, M. Dammak, S. Garcia-Granda, J. Solid State Chem. 277 (2019) 395–405, https://doi.org/10.1016/j. jssc.2019.06.036.

[52] O. Guesmia, M.S.M. Abdelbakyb, D. Martínez-Blanco, L. Ktari, S. García-Granda, M. Dammak, J. Inorganica Chim. Acta 496 (2019), 119033, https://doi.org/ 10.1016/j.ica.2019.119033.

[53] A. Moulahi, O. Guesmi, M.S.M. Abdelbaky, S. García-Granda, M. Dammak, J. Alloys Compd 898 (2022), 162956, https://doi.org/10.1016/j. jallcom.2021.162956.

[54] B.V. Nonius, Kappa CCD Server Software, Delft, The Netherlands, 1999.

[55] G.M. Sheldrick, A short history of SHELX, J. Acta Cryst. A 64 (2008) 112–122, https://doi.org/10.1107/S0108767307043930.

[56] G.M. Sheldrick, SHELXS-97: A Program for Crystal Structure, Gottingen University, Germany, 1997.

[57] L.J. Bourhis, O.V. Dolomanov, R.J. Gildea, J.A.K. Howard, H. Puschmann, J. Acta Cryst. A 71 (2015) 59–75, https://doi.org/10.1107/S2053273314022207.

[58] K. Brandenburg, M. Berndt, DIAMOND Version 2.1.b, Crystal Impact, Gb R, Bonn, Germany, 1999.

[59] B. Mennucci, J. Tomasi, J. Chem. Phys. 106 (1997) 5151–5158, https://doi.org/ 10.1063/1.473558.

[60] V. Barone, M. Cossi, J. Tomasi, J. Comput. Chem. 19 (1998) 404–417, https://doi. org/10.1002/(SICI)1096-987X(199803)19:4<404::AID-JCC3>3.0.CO;2-W.

[61] J. Tomasi, B. Mennucci, M.T. Cancès, J. Mol. Struct. 464 (1999) 211–226, https:// doi.org/10.1016/S0166-1280(98)00553-3.

[62] A.D. Becke, J. Phys. Rev. A: At. Mol. Opt. Phys. 38 (1988) 3098–3100, https://doi. org/10.1103/physreva.38.3098.

[63] C. Lee, W. Yang, R.G. Parr, J. Phys. Rev. B : Condens. Matter Mater. Phys. 37 (1988) 785–789, https://doi.org/10.1103/PhysRevB.37.785.

[64] A.D. Becke, J. Chem. Phys. 98 (1993) 5648–5652, https://doi.org/10.1063/ 1.464913.

[65] W.J. Hehre, L. Radom, P.v.R. Schleyer, J.A. Pople, J. Wiley, J. comput. Chem. 7 (1986) 379-379. doi: 10.1002/jcc.540070314.

[66] P.J. Hay, W.R. Wadt, J. Chem. Phys. 82 (1985) 270–283, https://doi.org/10.1063/ 1.448799.

[67] H.B. Schlegel, J. Comput. Chem. 3 (1982) 214–218, https://doi.org/10.1002/ jcc.540030212.

[68] H.B. Schlegel, J. Theor. Chem. Acc. 66 (1984) 333–340, https://doi.org/10.1007/ BF00554788.

[69] X. Li, M.J. Frisch, J. Chem. Theory Comput. 2 (2006) 835–839, https://doi.org/ 10.1021/ct050275a.

[70] F. Weinhold, C.R. Landis, Cambridge University Press, England, 2005. doi: 10.1017/CBO9780511614569.

[71] E.D. Glendening, A.E. Reed, J.E. Carpenter, Weinhold, F. NBO, Version 3.1, University of Wisconsin: Madison, WI, 2012.

[72] F. Furche, R. Ahlrichs, J. Chem. Phys. 117 (2002) 7433–7447, https://doi.org/ 10.1063/1.1508368.

[73] R.E. Stratmann, G.E. Scuseria, M.J. Frisch, J. Chem. Phys. 109 (1998) 8218-8224. doi: 10.1063/1.477483.

[74] R.L. Martin, J. Chem. Phys. 118 (2003) 4775–4777, https://doi.org/10.1063/ 1.1558471.

[75] S. Vyazovkin, A.K. Burnham, J.M. Criado, L.A. Pérez-Maqueda, C. Popescu, N. Sbirrazzuoli, J. Thermochim. Acta 520 (2011) 1–19, https://doi.org/10.1016/j. tca.2011.03.034.

[76] R.K. Matharu, Z. Charani, L. Ciric, U.E. Illangakoon, M. Edirisinghe, J. Appl. Polym. Sci. 135 (2018) 46368, https://doi.org/10.1002/app.46368.

[77] Z.H. Lin, C.H. Lee, H.Y. Chang, H.T. Chang, J. Chem. Asian 7 (2012) 930–934, https://doi.org/10.1002/asia.201101006.

[78] A.K. Jha, K. Prasad, K. Prasad, A.R. Kulkarni, J. Coll. Surf. B Biointerfaces 73 (2009) 219–223, https://doi.org/10.1016/j.colsurfb.2009.05.018.

[79] These Dhaou Maraii, Faculty of Sciences of Sfax-Tunisia, (2017).

[80] K. Azouzi, B. Hamdi, A. Ben Salah, J. Clust. Sci. 28 (2017) 3021–3334, https:// doi.org/10.1007/s10876-017-1274-1.

[81] A. Sakka, A. Jellali, B. Hamdi, M.S.M. Abdelbaky, H. Naïli, S. García-Granda, R. Zouari, J. Mol. Struct. 1198 (2019), 126867, https://doi.org/10.1016/j. molstruc.2019.07.114.

[82] S.K. Abdel-Aal, A.S. Abdel-Rahman, J. Cryst. Growth 457 (2017) 282–288, https:// doi.org/10.1016/j.jcrysgro.2016.08.006.

[83] A. Tounsi, B. Hamdi, R. Zouari, A. Ben Salah, J. Physica E 84 (2016) 384–394, https://doi.org/10.1016/j.physe.2016.07.025.

[84] A. Tounsi, S. Elleuch, B. Hamdi, R. Zouari, A. Ben Salah, J. Mol. Struct. 1141 (2017) 512-523. doi: 10.1016/j.molstruc.2017.04.003.

[85] A. Kessentini, M. Belhouchet, J.J. Suñol, Y. Abid, T. Mhiri, J. Spectrochim. Acta A 134 (2015) 28–33, https://doi.org/10.1016/j.jcrysgro.2016.08.006.

[86] C. Dubroca, J. Chem. Phys. Lett. 15 (1972) 207–210, https://doi.org/10.1016/ 0009-2614(72)80150-7.

[87] I. Iweibo, R.A. Oderinde, J.A. Faniran, J. Spectrochim. Acta A Mol. Biomol. Spectrosc. 38 (1982) 1–7, https://doi.org/10.1016/0584-8539(82)80170-0.

[88] M. Guruswamy, B. Ravindran, M. Mariappan, S.C. Mojumdar, J. Therm. Anal. Calorim. 100 (2010) 811–815, https://doi.org/10.1007/s10973-010-0760-6.

[89] A. Biswas, R. Bakthavatsalam, V. Bahadur, C. Biswas, B.P. Mali, S.S.K. Raavi, R. G. Gonnade, J. Kundu, J. Mater. Chem. C 9 (2021) 4351–4358, https://doi.org/ 10.1039/d0tc05752e.

[90] J. Dr, D.K.D. Kundu, Eur. J. Inorg. Chem. 2021 (2021) 4508–4520, https://doi.org/ 10.1002/ejic.202100685.

[91] M. Said, H. Boughzala, J. Mol. Struct. 1203 (2020), 127413, https://doi.org/ 10.1016/j.molstruc.2019.127413.

[92] M.S. Lassoued, M.S.M. Abdelbaky, A. Lassoued, S. Ammar, A. Gadri, A. Ben Salah, S. García-Granda, J. Mol. Struct. 11 (2017) 23, https://doi.org/10.1016/j. molstruc.2017.11.023.

[93] J.A. Huidobro, I. Iglesias, B.F. Alfonso, A. Espina, C. Trobajo, J.R. García, J. Chemometr. Intell. Lab. 151 (2016) 146–152, https://doi.org/10.1016/j. chemolab.2015.12.012.

[94] S. Ben Ali, A. Feki, V. Ferretti, M. Nasri, M. Belhouchet, J. R. Soc. Chem. 10 (2020) 35174–35184, https://doi.org/10.1039/d0ra05646d.

[95] A. Gannouni, I. Dridi, S. Elleuch, L. Jouffret, R. Kefi, J. Mol. Struct. 1250 (2022), 131804, https://doi.org/10.1016/j.molstruc.2021.131804.